Room temperature local nematicity in FeSe superconductor

R. J. Koch, T. Konstantinova, M. Abeykoon, A. Wang, C. Petrovic, Y. Zhu, E. S. Bozin, and S. J. L. Billinge

Room temperature local nematicity in FeSe superconductor

R. J. Koch[1,*], T. Konstantinova[1,2], M. Abeykoon[3], A. Wang[1,†],
C. Petrovic[1], Y. Zhu[1,2], E. S. Bozin[1], and S. J. L. Billinge[1,4]

[1]*Condensed Matter Physics and Materials Science Department,
Brookhaven National Laboratory, Upton, NY 11973, USA*
[2]*Department of Physics and Astronomy, Stony Brook University, Stony Brook, NY 11794, USA*
[3]*Photon Science Division, Brookhaven National Laboratory, Upton, NY 11973, USA* and
[4]*Department of Applied Physics and Applied Mathematics,
Columbia University, New York, NY 10027, USA*

(Dated: June 18, 2019)

We report pair distribution function measurements of the iron-based superconductor FeSe above and below the structural transition temperature. Structural analysis reveals a local orthorhombic distortion with a correlation length of about 4 nm at temperatures where an average tetragonal symmetry is observed. The analysis further demonstrates that the local distortion is larger than the global distortion at temperatures where the average observed symmetry is orthorhombic. Our results suggest that the low-temperature macroscopic nematic state in FeSe forms from an imperfect ordering of orbital-degeneracy-lifted nematic fluctuations which persist up to at least 300 K.

In high-temperature iron-based superconductors, nematicity, or C_4 to C_2 rotational symmetry breaking, is believed to be closely related to superconductivity as both are correlation-driven electronic instabilities which often coincide in the doping phase diagram [1]. The relationship is tantalizing but its nature remains unclear, as the two are frequently entwined with spin and orbital order [2, 3].

The emergence of nematicity is marked by a tetragonal to orthorhombic global symmetry breaking structural transition at T_s [4, 5] as well as a lifting of the degeneracy of electronic orbitals in the material. For example, in FeSe, angle-resolved photoemission spectroscopy (ARPES) studies have demonstrated that the $3d_{yz}$ and $3d_{xz}$ Fe-Fe molecular orbitals take on a 50 meV energy difference below $T_o = 90$ K. The observation of orbital degeneracy lifting (ODL) coincides with orbital ordering (OO) which in turn accompanies or indeed even drives [6] the global structural transition such that $T_o = T_s$ [7, 8].

Although the OO and structural transition occur concurrently, a notable discrepancy exists between their energy scales. The 50 meV orbital splitting corresponds to a temperature-scale of about 580 K rather than the 90 K of the transition. An alternative possibility is that the orbital degeneracy lifting happens at higher temperature, but the orbitals only order at T_s. This is similar to the case of $CuIr_2S_4$ [9], where a short-range ordered (SRO) ODL state was discovered to exist well above the OO temperature.

The well established lattice symmetry of FeSe above 90 K is tetragonal, with C_4 rotational symmetry about the c-axis. The low-temperature orthorhombic lattice in this system has C_2 symmetry along the same axis [10]. A structural signature for the existence of a SRO C_2 nematic phase above 90 K should manifest as a local, SRO orthorhombic (or similar) distortion, which does not order over long length scales. The x-ray atomic pair distribution function (xPDF) measurement provides a histogram of interatomic distances in a material, and as such is well suited for probing such local distortions [9, 11, 12]. Here we use xPDF to study an FeSe superconducting sample at temperatures both below and well above T_o and T_s.

In analogy with observations of ODL imposed structural distortions in $CuIr_2S_4$ [9], our xPDF study indicates a large orthorhombic distortion in FeSe up to 300 K, well above T_s where the average structure is tetragonal. Surprisingly, even at 84 K, just below the 90 K transition temperature, the local orthorhombic distortion is significantly larger in magnitude than the average crystallographic orthorhombicity that is recovered over large length scales, suggesting an imperfect long-range ordering of the local ODL state below T_s.

The nature of the local symmetry breaking is consistent with local degeneracy lifting of $3d_{yz}$ and $3d_{xz}$ orbitals associated with Fe-Fe bond formation. Our observation of a preformed local ODL broken symmetry state at high temperature portrays a picture where crystallization of the liquid-like orbital state occurs at the global symmetry breaking structural transition at T_s. This provides a rationale for the seemingly disparate energy scales involved. It can also explain the orbital degeneracy breaking above T_s implied by ARPES [13] and suggests that the ODL has a Jahn-Teller origin.

The FeSe sample was synthesized through chemical vapor transport method using a eutectic mix of KCl and $AlCl_3$ as the transport agent [14, 15]. Sample quality was validated by a temperature dependent resistivity characterization (Fig. S1 in Ref. [16]), which shows evidence for the structural phase transformation at $T_s = 90$ K and a robust superconducting transition below $T_c = 10$ K. Synchrotron x-ray total scattering experiments were conducted at the 28-ID-1 (PDF) beamline at the National Synchrotron Light Source-II

(NSLS-II) at Brookhaven National Laboratory (BNL). The sample was loaded into a 1 mm inner-diameter kapton capillary and data collected at 300 K and 84 K using a liquid N_2 cryostream. Measurements were carried out in the rapid acquisition pair distribution function (RaPDF) mode [17], with an x-ray energy of 74.69 keV (λ = 0.1660 Å). A two-dimensional (2D) PerkinElmer area detector was used, with a sample-to-detector distance of 204 mm determined by calibrating to a sample of known lattice parameter (Ni).

The 2D data were integrated and converted to intensity as a function of momentum transfer Q using the software FIT2D [18]. The program PDFGETX3 v2.0 [19] was used to correct, normalize, and Fourier transform the diffraction data to obtain the experimental xPDF, $G(r)$ up to a momentum transfer of $Q_{max} = 29$ Å^{-1} which was chosen as the best tradeoff between real-space resolution and noise in the data.

The average structure for FeSe is described by a tetragonal model at higher temperatures and an orthorhombic model at lower temperatures. The tetragonal model ($P4/nmm$ space-group, shown in Fig. 1) consists of FeSe slabs featuring a Fe square planar sublattice. Each Fe is coordinated by four Se creating layers of edge-shared $FeSe_4$-tetrahedra, regularly stacked along the **c** lattice direction [4, 5]. In this model, the asymmetric unit contains one FeSe formula unit, with Fe at $(0.25, 0.75, 0.0)$ and Se at $(0.25, 0.25, z)$. The lower temperature orthorhombic model ($Cmma$ space-group) is related to the tetragonal model through a rotation in the **a**-**b** plane and a rectangular distortion of the Fe sublattice [1]. Here, Fe sits at $(0.25, 0.0, 0.5)$ and Se at $(0.0, 0.25, z)$.

The xPDF data were fit with the PDFGUI [20] program using these two models (see Ref. [16] for details).

In Fig. 2 we show the PDF analysis results using the tetragonal model over the range $1.5 < r < 50$ Å. An abridged r-range is shown for clarity and the resulting structural parameters are summarized in Table I. The fit is acceptable, with an overall $R_w = 0.08$, suggesting that the tetragonal model adequately describes the average structure of FeSe at 300 K. However, a feature at ~ 3.9 Å in the local structure portion of the PDF is not well reproduced by the tetragonal model. The misfit on this peak is associated with a larger R_w of 0.11 over the range $1.5 < r < 5$ Å, compared to $R_w = 0.06$ over the range $5 < r < 15$ Å, as highlighted in Fig. 2.

The PDF misfit in a single low$-r$ peak (Fig. 2) is reminiscent of the fingerprint of a SRO ODL state in $CuIr_2S_4$ [9]. In that system, a large misfit was observed in the first Ir-Ir PDF peak at $r = 3.5$ Å when the PDF was fit with the reported cubic average structure, with an absence of significant misfit at other places in the PDF. This discrepancy was explained by the presence of fluctuating local symmetry-broken tetragonal domains present in the average cubic phase, that act as a precursor for the long-range ordered symmetry broken ground-state seen
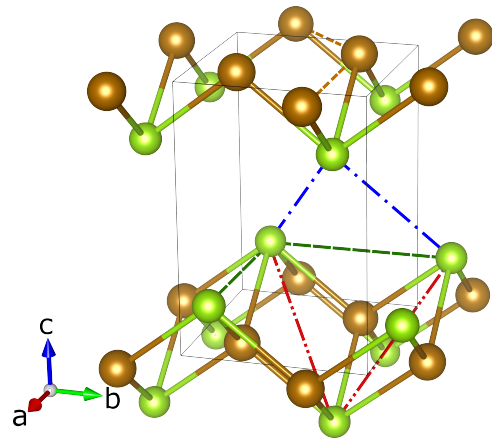

FIG. 1. Perspective view of the FeSe structure with tetragonal symmetry. Iron is shown in brown, and selenium in green. Pair distances constrained by tetragonal symmetry to be identical are highlighted by dashed lines of the same color. Tetragonal symmetry allows only a single Fe-Fe pair distance (brown dashed lines), and the orthorhomic distortion allows these distances to differentiate. The three unique Se-Se pair distances shown by red, green, and blue dashed lines become five distinct Se-Se pairs within the orthorhombic symmetry.
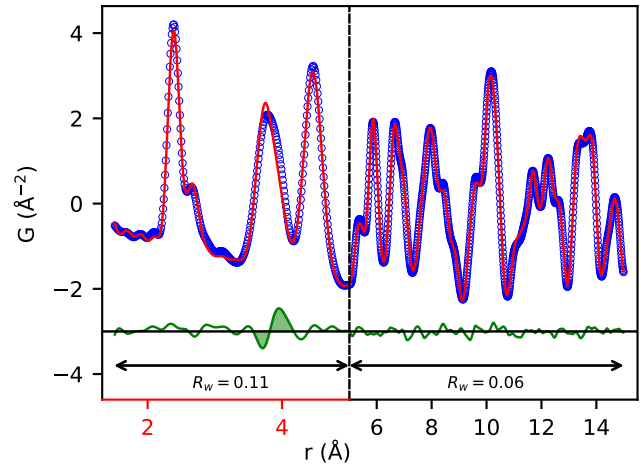

FIG. 2. The signature of local nematicity. PDF of best-fit model (red solid line) to observed data (open circles) from FeSe at 300 K, fitted up to $r = 50$ Å using the tetragonal model (overall $R_w = 0.08$). The fit is presented over the abbreviated range $1.5 < r < 15$ Å for clarity. The difference curve is shown displaced below (green solid line), and shaded to highlight the signature of local nematicity. R_w values over selected abbreviated r-ranges are presented to highlight low-r misfit. Different coloring of the x-axes of two panels signals that the scales are distinct to highlight the signal at low-r. The y-axis scales are preserved between the two panels. Importantly, there is also a subtle misfit of the Fe-Fe peak at 2.7 Å (see text for details).

TABLE I. Structural parameters and fit details for the FeSe sample at 300 K, obtained from PDF analysis using either the tetragonal or orthrhombic model. Colors in pair distances are consistent with dashed lines in Fig. 1

Parameter	Tetragonal	Orthorhombic
r-range (Å)	1.5–50	1.5–5.0
R_w	0.08	0.04
a (Å)	3.771	5.32
b (Å)	–	5.41
c (Å)	5.520	5.50
z	0.266	0.235
r(Fe–Se) (Å)	2.391	2.391
r(Fe–Fe) (Å)	2.667	2.661
	–	2.710
r(Se–Se) (Å)	3.710	3.709
	–	3.742
	3.771	3.795
	3.970	3.944
	–	3.974

at low temperature in the CuIr$_2$S$_4$ system.

In our FeSe system the corresponding reminiscent misfit feature occurs at $r = 3.9$ Å corresponding to a composite peak originating primarily from Se-Se nearest-neighbor (NN) correlations. The FeSe tetragonal model allows for three distinct Se-Se NN distances. The first set of NN Se-Se interatomic vectors spans the sheet created by the FeSe$_4$-tetrahedra between Se pairs with distinct z coordinates (red dashed lines in Fig. 1). The second spans the space between different sheets, again involving Se pairs with distinct z coordinates (blue dashed lines in Fig. 1). The third connects Se pairs with identical z coordinates, either fully above or below the Fe species in the same layer (green dashed lines in Fig. 1).

These symmetry constraints are lifted for some but not all of these interatomic vectors when the orthorhombic distortion occurs. The NN Se-Se interatomic vectors that connect Se ions with distinct z coordinates, represented by red and blue dashed lines in Fig. 1, all lie along the orthorhombic unit cell axes (i.e., the basal-plane projection of the interatomic vectors are parallel to a and b, respectively). The orthorhombic distortion allows these pair distances to become distinct, with the magnitude of their difference dictated by the magnitude of the orthorhombic distortion. On the other hand, the NN Se-Se interatomic vectors with zero z component, represented by green dashed lines in Fig. 1, are parallel to the diagonals of the orthorhombic a-b plane and they remain identical following the orthorhombic distortion. The reduction of symmetry associated with the orthorhombic

distortion therefore results in an increase from three to 5 distinct Se-Se NN distances. The feature at $r = 3.9$ Å also contains a Fe-Fe next nearest neighbor (NNN) contribution, but this peak is smaller than the Se-Se contributions by a factor of about five, and the orthorhombic distortion does not split the two Fe-Fe NNN distances, as they span the unit cell diagonals.

The feature at ~ 3.9 Å in the difference curve in Fig. 2 suggests intensity is shifted to the right in the measured PDF compared to the model. This indicates that the tetragonal model PDF under-represents higher-r Se-Se NN pair correlations, while lower-r Se pair correlations are over-represented.

Drawing from the previously mentioned CuIr$_2$S$_4$ case [9], we seek an explanation in terms of a SRO locally orbital degeneracy lifted (SRO-ODL) state which persists to temperatures well above the observed long-range OO temperature T_o. In CuIr$_2$S$_4$, the local structure of the material in the SRO-ODL state was well explained by the symmetry broken model, while the high-r region was consistent with the high-temperature non-symmetry-broken structural model. We therefore followed a similar analysis strategy as adopted in the CuIr$_2$S$_4$ case.

As mentioned, long-range OO in FeSe manifests structurally as a tetragonal to orthorhombic transformation, which involves an increase in the number of distinct Se-Se NN distances. Our analysis applying the low temperature orthorhombic model to the low-r ($1.5 < r < 5$ Å) region of the 300 K PDF is shown in Fig. 3, with resulting structural parameters presented in Table I. This model successfully removes the reminiscent misfit feature that is observed in this r-region with the tetragonal model, yielding an R_w nearly 3× lower than the tetragonal model, ($R_w = 0.04$ vs. 0.11) over the range $1.5 < r < 5$ Å. This strongly suggests that at 300 K the local structure is orthorhombic and is a SRO-ODL state.

Compared to the average structure, the orthorhombic distortion does not alter the Fe-Se distance, but does split the NN Se-Se and NN Fe-Fe pair distances significantly, while also shifting them to higher-r. The misfit in Fig. 2 is more apparent in the NN Se-Se PDF peak at ~ 3.9 Å rather than the NN Fe-Fe PDF peak at ~ 2.7 Å due to the stronger scattering power of Se and a larger Se-Se multiplicity, resulting in a peak that is roughly four-times stronger than the NN Fe-Fe peak.

A similar sized distortion in the Fe and Se sub-lattices thus results in a much larger signature in the difference curve associated with Se-Se features. However, and importantly, careful inspection of the Fe-Fe peak at 2.7 Å, evident as a well resolved shoulder to the Fe-Se peak in Fig. 2, indicates that this peak is observably broader in the data than the model. This misfit, although subtle, is consistent with the presence of an ODL state in the Fe-Fe sublattice. While such a misfit alone could easily escape attention, the broader context of the large residual at ~ 3.9 Å highlights this region.
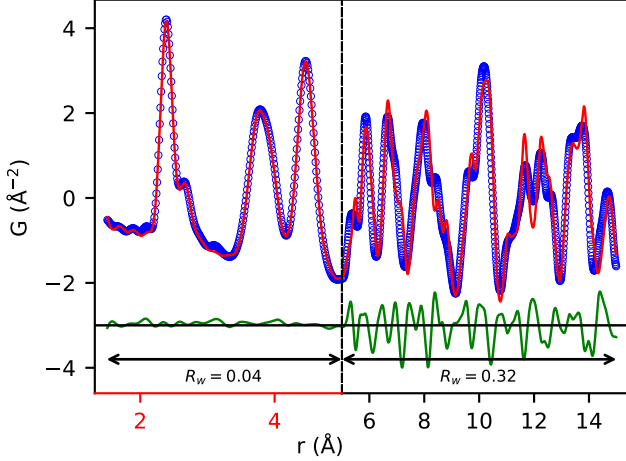
FIG. 3. PDF of best-fit model (red solid line) and observed data (open circles) from FeSe at 300 K, fitted up to $r = 5$ Å using orthorhombic (nematic) symmetry constraints ($R_w = 0.04$). The difference curve is shown displaced below (green solid line). R_w values over selected r-ranges are presented to highlight the discrepancy between the optimal local structure and the observed average structure. Different coloring of the x-axes of two panels signals that the scales are distinct to highlight the signal at low-r. The y-axis scales are preserved between the two panels. The orthorhombic model provides observably better account of the Fe-Fe NN PDF peak as compared to the tetragonal model (Fig. 2)
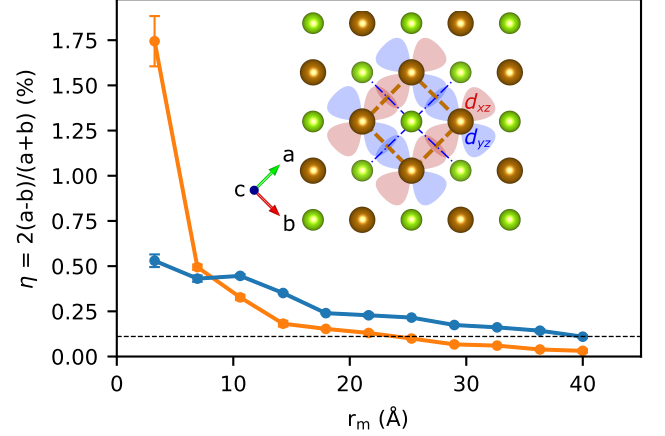

FIG. 4. The measured orthorhombic distortion obtained by using an orthorhombic model over a narrow r-range, η, is plotted vs the PDF fit window center, r_m, for data measured at 300 K (orange line) and 84 K (blue line). The value of η at 84 K as extracted from the average structure is represented by the dashed horizontal line. Inset is a top view of the FeSe crystal structure, schematically showing the projected orientations of the Fe $3d_{yz}$ and $3d_{xz}$ orbitals implicated in this work and elsewhere. Atom and dashed line colors are consistent with Fig. 1 and the axes labels are consistent with the orthorhombic setting. Full PDF fits associated with the distortion magnitudes in this plot are shown in Fig. S2 in Ref. [16]

As in the $CuIr_2S_4$ case, if we calculate the PDF of the orthorhombic model, which reproduces the low-r region well, over a much wider r-range (up to 15 Å), it results in a poor agreement to the measured PDF compared to the non-symmetry broken tetragonal model (Fig. 3, $R_w = 0.32$ for $5 < r < 15$ Å compared to $R_w = 0.06$ for the tetragonal model over this range). This implies that the distortion has orthorhombic short-range character.

Given that we have found local orthorhombic domains in a globally tetragonal crystal, we would like to extract the size, or structural coherence, of the domains. To do this we use box-car style PDF fits [21, 22] where the fits are carried out over a number of variable r-range regions individually. The protocol represents an extension of the fitting shown in Fig. 3, wherein the "box-car" consisted of the r-range of 1.5-5 Å, and a centroid $r_m = 1.75$ Å. Each distinct r-range fit then provides structural information relevant to a distinct distance window, allowing for a quantification of the variation of local structure as a function of r (the correlation length of local features). The orthorhombic distortion η as a function of the box-car centroid, r_m, is shown in Fig. 4, demonstrating the robustness of the approach (see Fig. S2 in Ref. [16])

Surprisingly, our analysis reveals that the local distortion above T_s is about 1.75 %, more than 3× larger than any observed distortion in the average structure be-

low T_s. The magnitude of the measured distortion drops rapidly with increasing r (Fig. 4) until, at length scales greater than 40 Å, it is effectively zero and the average tetragonal structure is recovered.

Interestingly, even below T_s (at $T = 84$ K) the local orthorhombicity is larger than that observed in the average structure at this temperature, represented by the dashed horizontal line in Fig. 4. At this temperature, the local distortion also decreases with increasing r, converging to the measured average orthorhombic structure at length scales greater than 40 Å. Based on the proposed SRO-ODL explanation, the persistence of a larger-than-average local orthorhombicity below T_s suggests that the long-range ordering of the ODL state is not perfect.

The xPDF results presented here build on and extend previous studies [23, 24] showing similarly local C_4 symmetry breaking in the 122 family of iron pnictide superconductors, suggesting that such fluctuations may be widespread.

Further, our findings provide a direct structural rationale for anomalous line width and splitting observed in NMR spectra [25] as well as unexpected energy gaps observed in the electronic spectra [13, 26, 27] pointing towards electronic non-degeneracy in FeSe well above T_s. The $3d_{yz}$ and $3d_{xz}$ Fe orbitals implicated in this local degeneracy lifting are oriented along the distorted or-

thorhombic direction (see e.g. Fig. 4 inset) and participate in orbital-selective Cooper pairing [28, 29] enhanced by nematic order [30]. Thus the xPDF discovery of a local ODL state deep in the high temperature tetragonal regime not only defines a local structural fingerprint of the fluctuating nematic state, but also serves to reinforce the role of the orbital sector and its coupling to structure within the physics of iron-based superconductors. Local orbital overlaps governed by nematic fluctuations appear to be essential for slow dynamic correlations in FeSe and related materials [31, 32]. Our observation of a broken symmetry state at high temperature suggests that the global symmetry breaking structural transition at T_s occurs through crystallization of the preformed liquid-like orbital state, a description which challenges present understanding of this system and invites further theoretical considerations.

To that effect, it will be of particular interest to explore the evolution of this local ODL state away from the FeSe parent, across the phase diagrams of e.g. $FeSe_{1-x}S_x$ and $FeSe_{1-x}Te_x$ and in the regime where long range symmetry breaking transition is not observed at any temperature. Such studies would further inform the debate of the importance of nematic fluctuations for the superconductivity itself.

* rkoch@bnl.gov

† Present address: School of Physics, Chongqing University, Chongqing 400044, China

[1] A. E. Böhmer and A. Kreisel, Journal of Physics Condensed Matter **30**, 023001 (2018), ISSN 1361648X, URL http://stacks.iop.org/0953-8984/30/i=2/a=023001?key=crossref.ba883e5813404f0303acc79d5e40c783.

[2] R. M. Fernandes, A. V. Chubukov, and J. Schmalian, Nature Physics **10**, 97 (2014), ISSN 17452473.

[3] Q. Si, R. Yu, and E. Abrahams, Nature Reviews Materials **1**, 16017 (2016), ISSN 2058-8437, URL https://www.nature.com/articles/natrevmats201617.

[4] F. C. Hsu, J. Y. Luo, K. W. Yeh, T. K. Chen, T. W. Huang, P. M. Wu, Y. C. Lee, Y. L. Huang, Y. Y. Chu, D. C. Yan, et al., Proceedings of the National Academy of Sciences **105**, 14262 (2008), ISSN 0027-8424, URL http://www.pnas.org/cgi/doi/10.1073/pnas.0807325105.

[5] S. Hosoi, K. Matsuura, K. Ishida, H. Wang, Y. Mizukami, T. Watashige, S. Kasahara, Y. Matsuda, and T. Shibauchi, Proceedings of the National Academy of Sciences **113**, 8139 (2016), ISSN 0027-8424, URL http://arxiv.org/abs/1604.00184%0Ahttp://dx.doi.org/10.1073/pnas.1605806113.

[6] S. H. Baek, D. V. Efremov, J. M. Ok, J. S. Kim, J. van den Brink, and B. Büchner, Nature Materials **14**, 210 (2015), ISSN 1476-1122, 1476-4660, URL http://www.nature.com/articles/nmat4138.

[7] T. Shimojima, Y. Suzuki, T. Sonobe, A. Nakamura, M. Sakano, J. Omachi, K. Yoshioka, M. Kuwata-Gonokami, K. Ono, H. Kumigashira, et al., Physical Review B - Condensed Matter and Materials Physics **90**, 121111 (2014), ISSN 1550235X, URL https://journals.aps.org/prb/pdf/10.1103/PhysRevB.90.121111https://link.aps.org/doi/10.1103/PhysRevB.90.121111.

[8] T. M. McQueen, A. J. Williams, P. W. Stephens, J. Tao, Y. Zhu, V. Ksenofontov, F. Casper, C. Felser, and R. J. Cava, Physical Review Letters **103** (2009), ISSN 0031-9007, 1079-7114, URL https://link.aps.org/doi/10.1103/PhysRevLett.103.057002.

[9] E. S. Bozin, W. G. Yin, R. J. Koch, M. Abeykoon, Y. S. Hor, H. Zheng, H. C. Lei, C. Petrovic, J. F. Mitchell, and S. J. L. Billinge, arXiv:1901.10104 [cond-mat] (2019), arXiv: 1901.10104, URL http://arxiv.org/abs/1901.10104.

[10] K. Kothapalli, A. E. Böhmer, W. T. Jayasekara, B. G. Ueland, P. Das, A. Sapkota, V. Taufour, Y. Xiao, E. Alp, S. L. Bud'ko, et al., Nature Communications **7** (2016), ISSN 2041-1723, URL http://www.nature.com/articles/ncomms12728.

[11] S. J. L. Billinge and M. G. Kanatzidis, Chem. Commun. **7**, 749 (2004), URL http://doi.org/10.1039/b309577k.

[12] T. Egami and S. J. L. Billinge, Underneath the Bragg peaks: structural analysis of complex materials (Elsevier, Amsterdam, 2012), 2nd ed., URL http://store.elsevier.com/product.jsp?lid=0\&iid=73\&sid=0\&isbn=9780080971414.

[13] P. Zhang, T. Qian, P. Richard, X. P. Wang, H. Miao, B. Q. Lv, B. B. Fu, T. Wolf, C. Meingast, X. X. Wu, et al., Phys. Rev. B **91**, 214503 (2015), URL https://link.aps.org/doi/10.1103/PhysRevB.91.214503.

[14] R. Hu, H. Lei, M. Abeykoon, E. S. Božin, S. J. L. Billinge, J. B. Warren, T. Siegrist, and C. Petrovic, Physical Review B - Condensed Matter and Materials Physics **83**, 1 (2011), ISSN 10980121.

[15] D. Chareev, E. Osadchii, T. Kuzmicheva, J.-Y. Lin, S. Kuzmichev, O. Volkova, and A. Vasiliev, CrystEngComm **15**, 1989 (2013), ISSN 1466-8033, URL https://pubs.rsc.org/en/content/articlelanding/2013/ce/c2ce26857d.

[16] See Supplemental Material at [URL will be inserted by publisher] for electrical transport properties, details on the xPDF analysis, and Refs. [20, 33, 34].

[17] P. J. Chupas, K. W. Chapman, and P. L. Lee, J. Appl. Crystallogr. **40**, 463 (2007).

[18] A. P. Hammersley, S. O. Svenson, M. Hanfland, and D. Hauserman, High Pressure Res. **14**, 235 (1996).

[19] P. Juhás, T. Davis, C. L. Farrow, and S. J. L. Billinge, J. Appl. Crystallogr. **46**, 560 (2013), URL http://dx.doi.org/

10.1107/S0021889813005190.

[20] C. L. Farrow, P. Juhás, J. Liu, D. Bryndin, E. S. Božin, J. Bloch, T. Proffen, and S. J. L. Billinge, J. Phys: Condens. Mat. **19**, 335219 (2007), URL http://iopscience.iop.org/0953-8984/19/33/335219/.

[21] X. Qiu, T. Proffen, J. F. Mitchell, and S. J. L. Billinge, Phys. Rev. Lett. **94**, 177203 (2005), URL http://journals.aps.org/prl/abstract/10.1103/PhysRevLett.94.177203.

[22] B. E. S., K. R. Knox, P. Juhás, Y. S. Hor, J. F. Mitchell, and S. J. L. Billinge, Scientific Reports **4**, 4081 (2014), ISSN 2045-2322, URL https://www.nature.com/articles/srep04081.

[23] T. Iye, M.-H. Julien, H. Mayaffre, M. Horvatić, C. Berthier, K. Ishida, H. Ikeda, S. Kasahara, T. Shibauchi, and Y. Matsuda, Journal of the Physical Society of Japan **84**, 043705 (2015), ISSN 0031-9015, URL https://journals.jps.jp/doi/full/10.7566/JPSJ.84.043705.

[24] B. A. Frandsen, K. M. Taddei, D. E. Bugaris, R. Stadel, M. Yi, A. Acharya, R. Osborn, S. Rosenkranz, O. Chmaissem, and R. J. Birgeneau, Phys. Rev. B **98**, 180505 (2018), URL https://link.aps.org/doi/10.1103/PhysRevB.98.180505.

[25] P. Wiecki, M. Nandi, A. E. Böhmer, S. L. Bud'ko, P. C. Canfield, and Y. Furukawa, Physical Review B **96**, 180502 (2017), URL https://link.aps.org/doi/10.1103/PhysRevB.96.180502.

[26] Y. C. Wen, K. J. Wang, H. H. Chang, J. Y. Luo, C. C. Shen, H. L. Liu, C. K. Sun, M. J. Wang, and M. K. Wu, Physical Review Letters **108** (2012), ISSN 0031-9007, 1079-7114, URL https://link.aps.org/doi/10.1103/PhysRevLett.108.267002.

[27] P. S. Wang, P. Zhou, S. S. Sun, Y. Cui, T. R. Li, H. Lei, Z. Wang, and W. Yu, Physical Review B **96** (2017), ISSN 2469-9950, 2469-9969, URL https://link.aps.org/doi/10.1103/PhysRevB.96.094528.

[28] P. O. Sprau, A. Kostin, A. Kreisel, A. E. Böhmer, V. Taufour, P. C. Canfield, S. Mukherjee, P. J. Hirschfeld, B. M. Andersen, and J. C. Davis, Science **357**, 75 (2017), ISSN 10959203, URL http://science.sciencemag.org/content/357/6346/75http://www.sciencemag.org/lookup/doi/10.1126/science.aal1575.

[29] A. Kostin, P. O. Sprau, A. Kreisel, Y. X. Chong, A. E. Böhmer, P. C. Canfield, P. J. Hirschfeld, B. M. Andersen, and J. C. Davis, Nature Materials **17**, 869 (2018), ISSN 14764660, URL https://www.nature.com/articles/s41563-018-0151-0http://www.nature.com/articles/s41563-018-0151-0.

[30] R. Yu, J.-X. Zhu, and Q. Si, Phys. Rev. Lett. **121**, 227003 (2018), URL https://link.aps.org/doi/10.1103/PhysRevLett.121.227003.

[31] I. Zaliznyak, A. T. Savici, M. Lumsden, A. Tsvelik, R. Hu, and C. Petrovic, Proceedings of the National Academy of Sciences **112**, 10316 (2015), ISSN 0027-8424, https://www.pnas.org/content/112/33/10316.full.pdf, URL https://www.pnas.org/content/112/33/10316.

[32] T. Konstantinova, L. Wu, M. Abeykoon, R. J. Koch, A. F. Wang, R. K. Li, X. Shen, J. Li, J. Tao, I. A. Zaliznyak, et al., Phys. Rev. B **99**, 180102 (2019), URL https://link.aps.org/doi/10.1103/PhysRevB.99.180102.

[33] T. Proffen and S. J. L. Billinge, J. Appl. Crystallogr. **32**, 572 (1999), URL http://www.pa.msu.edu/cmp/billinge-group/programs/discus/pdffit.html.

[34] B. H. Toby and T. Egami, Acta Crystallogr. A **48**, 336 (1992).